Formation and evolution of roll patterns in optical parametric oscillators

Gian-Luca Oppo
Department of Physics, University of Strathclyde, 107 Rottenrow, Glasgow G4 0NG, Scotland, United Kingdom

Massimo Brambilla and Luigi A. Lugiato
Department of Physics, University of Milano, Via Celoria 16, Milano 20133, Italy

(Received 1 June 1993)

We study pattern formation in a degenerate optical parametric oscillator (OPO) by including diffractive effects due to the propagation in the optical cavity. The solution of zero amplitude for the OPO signal is found to be unstable to periodically modulated perturbations whenever the detuning parameter of the signal field is negative. A comparison between analytical solutions and numerical simulations for the roll structure shows excellent agreement for a wide range of input amplitudes. The threshold for the appearance of rolls is lower than the usual OPO threshold obtained in the plane-wave limit, especially for large detunings. When the input power is increased, roll patterns lose stability, leading to filamentation and optical turbulence.

PACS number(s): 42.65.−k, 47.20.Ky, 05.45.+b

Optical parametric oscillators (OPO's) in Fabry-Perot cavities have been extensively studied both theoretically and experimentally. For example, the parametric down-conversion allows one to tune input lasers for broad ranges of frequencies (see Ref. [1] and references therein). OPO's have also been shown to produce high level of squeezing [2], which has been recently related to the appearance of transverse structures [3], the subject of this paper.

Pattern formation in nonlinear optics is a rapidly growing subject. Seminal works about optically bistable systems [4], lasers [5] and Kerr slices [6] paved the way for observation and interpretation of transverse patterns dynamics in a broad range of active [7] and passive [8] devices. Here we focus on a different kind of nonlinearity leading to parametric down-conversion, coupled with diffraction during propagation in an optical cavity. Earlier studies of pattern formation during three-wave nonlinear mixing have already shown the existence of optical defects [9] originally introduced in the context of laser dynamics [10]. Our main result concerns modulational instabilities which lower the plane-wave threshold for the operation of the OPO. Rolls structures are found both analytically and numerically and are shown to be stable for a wide range of the parameter space. Their formation is associated with an asymmetry between the two sides of the resonance as rolls appear only for frequency of the signal mode smaller than half input laser frequency (negative detunings). Here we focus on the spatiotemporal dynamics of roll structures leaving the case of positive detunings to future analysis. By increasing the pump intensity, rolls first bend at sharp angles (zigzag mechanism) and later lose stability, leading to the formation of dislocations. Moreover, the system tries to recover both the translational and the cylindrical symmetries previously broken by the formation of rolls, via filamentation and optical turbulence.

We generalize a model for a degenerate OPO in a Fabry-Pérot cavity introduced by Drummond, McNeil, and Walls [11] to include diffractive effects during free propagation. We consider an optical cavity with plane mirrors, containing a nonlinear $\chi^{(2)}$ medium which converts a field of frequency ω_L into a field of frequency $\omega_L/2$, and vice versa. Two longitudinal modes of the cavity, with frequency ω_0 and ω_1, are close to resonance with the field frequencies ω_L and $\omega_L/2$, respectively. A coherent continuous wave field of frequency ω_L is injected into the laser cavity.

We assume the validity of the paraxial approximation, the mean-field limit, and the single longitudinal mode approximation for the two fields. By following a procedure substantially identical to that of Ref. [5] but for plane instead of spherical mirrors, we derive the following set of dynamical equations:

$$\partial_t A_0=\gamma_0[-(1+i\Delta_0)A_0+E-A_1^2+ia_0\nabla^2 A_0]\ , \quad (1)$$

$$\partial_t A_1=\gamma_1[-(1+i\Delta_1)A_1+A_1^* A_0+ia_1\nabla^2 A_1]\ , \quad (2)$$

where $A_0(x,y,t)$ and $A_1(x,y,t)$ are the normalized slowly varying envelopes for the pump and signal fields, respectively; x and y denote the Cartesian coordinates of the plane orthogonal to the direction of propagation (z) and the normalization is the same used in [12], for example, γ_0 and γ_1 are the cavity decay rates of the two field modes defined as

$$\gamma_0=\frac{cT_0}{\Lambda},\quad \gamma_1=\frac{cT_1}{\Lambda}\ , \quad (3)$$

where T_0 and T_1 are the transmittivities of the mirrors at the pump and signal frequencies, Λ is the round-trip cavity length, and

$$\Delta_0=\frac{\omega_0-\omega_L}{\gamma_0},\quad \Delta_1=\frac{\omega_1-\omega_L/2}{\gamma_1} \quad (4)$$

are the detuning parameters for the pump and signal

fields, respectively. ∇^2 denotes the transverse Laplacian operator

$$\nabla^2=\frac{\partial^2}{\partial x^2}+\frac{\partial^2}{\partial y^2}\ , \tag{5}$$

which describes diffraction while the coefficients a_0,a_1 are given by

$$a_0=\frac{c}{2k_z\gamma_0},\quad a_1=\frac{c}{k_z\gamma_1} \tag{6}$$

where c is the velocity of light and k_z is the longitudinal component of the wave vector of the field of frequency ω_L. The parameter E, here considered real and positive, is the normalized amplitude of the input field. We have initially considered E spatially homogeneous to simulate the effects of a plane input wave. In the last part of the paper, we briefly consider the action of a nonplanar input beam in order to show the generality and robustness of our results.

We first consider the uniform stationary solution (i.e., independent of x,y,t) which characterizes the OPO below the threshold of signal generation; it is given by

$$A_0^{\rm st}=\frac{E(1-i\Delta_0)}{1+\Delta_0^2},\quad A_1^{\rm st}=0\ . \tag{7}$$

In the framework of the plane-wave model, where the terms containing ∇^2 in (1) and (2) are neglected, the state (7) becomes unstable to uniform perturbations for input amplitudes larger than

$$E_{\rm thr}^{\rm PW}=\sqrt{(1+\Delta_0^2)(1+\Delta_1^2)}\ . \tag{8}$$

In contrast to Refs. [11] and [12] where details of the stability analysis of the plane wave case are provided, we focus here on spatially modulated perturbations. It is then convenient to introduce a new variable $B\equiv A_0-A_0^{\rm st}$ and to separate Eqs. (1) and (2) in linear and nonlinear terms

$$\partial_t B=\gamma_0[-(1+i\Delta_0)B+ia_0\nabla^2 B]-\gamma_0 A_1^2\ , \tag{9}$$

$$\partial_t A_1=\gamma_1[-(1+i\Delta_1)A_1+A_1^* A_0^{\rm st}+ia_1\nabla^2 A_1]+\gamma_1 A_1^* B\ . \tag{10}$$

By dropping the last term in both Eqs. (9) and (10), we obtain the equations which govern the linear stability of the solution (7). The generic solution of these linearized equations is a linear combination of solutions of the form

$$\begin{bmatrix} B \\ A_1 \end{bmatrix}\propto e^{\lambda(k)t}e^{i(k_x x+k_y y)}\ , \tag{11}$$

where k_x,k_y are the transverse components of the wave vector and $\lambda(k)$ are the four eigenvalues of the linearized problem, which depend on $k=(k_x^2+k_y^2)^{1/2}$ and on the parameters of the system. The threshold for signal generation corresponds to the value of the input field E such that an eigenvalue $\lambda(k)$ vanishes and is given by

$$E=\{(1+\Delta_0^2)[1+(\Delta_1+\tilde{k}^2)^2]\}^{1/2} \tag{12}$$

with

$$\tilde{k}=a_1^{1/2}k\ . \tag{13}$$

When $\Delta_1\geq 0$, the minimum of the function (12) is for $\tilde{k}=0$, which means that the signal field arises as a uniform plane wave in the axial direction [see Eq. (8)]. On the other hand, for $\Delta_1<0$ (the case of interest in this paper), the function (12) is plotted in Fig. 1 and presents a minimum for a well-defined transverse wave vector given by

$$\tilde{k}_c=\sqrt{-\Delta_1}\ . \tag{14}$$

which is independent of the pump detuning Δ_0. The critical value of the input energy for this modulational instability (i.e., the threshold for signal generation) is readily obtained from Eq. (12):

$$E_C=\sqrt{1+\Delta_0^2}\ , \tag{15}$$

which is consistently lower than $E_{\rm thr}^{PW}$ especially for large detunings $|\Delta_1|$. This effect may have important consequences on the experimental side where tunability of input lasers requires low threshold of operation for OPO crystals.

Note that the phenomenon which makes the OPO threshold independent of the signal detuning for negative values of Δ_1 is analogous to the origin of phase traveling-wave solutions at threshold in lasers as described in Ref. [13] in the analysis of a model introduced in [14]. For both OPO's and lasers, diffraction coupled with the material nonlinearity leads to an off-axis emission that compensates for the off-resonance condition. Such a phenomenon is confined to one side of the resonance only. At difference from the laser case, however, numerical simulations of the OPO equations (1) and (2) above the threshold (15) show the appearance of roll solutions corresponding to periodic modulation of the output intensity (see Fig. 2, solid line). The characteristic wave vector of the spatial modulation is found to be k_c, in excellent agreement with Eq. (14). Numerical simulations

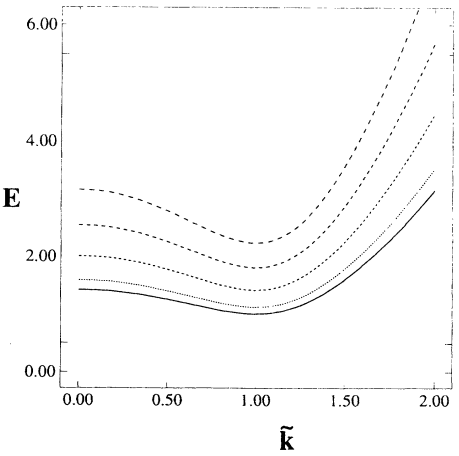

FIG. 1. The threshold input amplitude versus the roll wave vector for $\gamma_0=\gamma_1=1.0$, $\Delta_1=-1.0$, and five values of Δ_0. The values of Δ_0 are from the bottom curve to the top 0.0, 0.5, 1.0, 1.5, and 2.0, respectively.

have been performed by using lattice spacing equal to 0.3 on square grids of 200×200 sites and on rectangular girds of 800×50 sites to check that the periodic boundary conditions did not affect the formation and evolution of roll patterns.

The physical reason for the appearance of a roll pattern instead of a phase traveling wave is that the parametric down-conversion process gives rise to simultaneous emission of *two* symmetric traveling waves because of momentum conservation. The superposition of these traveling waves originates the roll configuration.

An exact form of the roll solution is unfortunately not available. However, a careful application of perturbation expansions allows us to find close approximations [15] whose range of validity extends to values of the input intensity far higher than the threshold specified by (15). For simplicity we analyze the case of equal decay rates for the field modes (i.e., $\gamma_0=\gamma_1$), but the calculations are easily extended to the general case. Moreover, the axes of the transverse plane have been chosen parallel and perpendicular to the rolls in order to simplify the final formulas. It is important to stress here that the following analysis is two dimensional in space. Equations (9) and (10) have an optimal form for a perturbation expansion close to threshold. By solving the equations related to the linear operator, one finds that there is no contribution at first order for the field B while the solution for the field A_1 is

$$A_1=\epsilon[\Delta_0+i(1-\sqrt{1+\Delta_0^2})]\cos(k_c x)\ , \tag{16}$$

where the smallness parameter ϵ remains to be evaluated by the solvability condition which fixes the Fredholm alternative [15]. To find ϵ we have to evaluate both second and third order of the expansion as the solvability condition vanishes at lower orders. The first order term (16) to the OPO signal yields a smaller correction on the pump field which can be evaluated at the next order in the perturbation expansion

$$B=\epsilon^2[\alpha+\beta\cos^2(k_c x)]\ , \tag{17}$$

where

$$\alpha=\frac{2a_0k_c^2(\Delta_0+i)}{1+\Delta_0^2}\beta\ , \tag{18}$$

$$\beta=\frac{2(1-\sqrt{1+\Delta_0^2})[1-\Delta_0^2-4\Delta_0a_0k_c^2-2i(\Delta_0+2a_0k_c^2)]}{1+(\Delta_0+4a_0k_c^2)^2}\ . \tag{19}$$

The expansion is then closed by evaluating the smallness parameter ϵ by use of the solvability condition at the third order

$$\epsilon=\pm\left|\frac{E-\sqrt{1+\Delta_0^2}}{(2a_0k_c^2+\frac{3\Delta_0}{4})\mathrm{Re}(\beta)-\frac{3}{4}\mathrm{Im}(\beta)}\right|^{1/2}\ . \tag{20}$$

It is easy to verify from Eq. (20) that the denominator is always positive, so that the bifurcation leading to rolls in OPO's is always supercritical, i.e., the roll pattern exists and is stable immediately above threshold. A comparison between the previously analytical calculations and the numerical simulations is shown in Figs. 2 and 3 for both the signal A_1 and the pump field A_0. The agreement is spectacular even for input amplitudes E far from the predicted threshold (15). An explanation of this fact is that expression (17) is actually an exact solution of Eq. (9) once the signal field has the form (16). This means that well above threshold the amplitude of spatial modulation of the signal field remains larger than that of the pump field, in agreement with the perturbation expansion.

At larger values of the input amplitude, a second spatial instability develops in a direction perpendicular to the rolls leading to zigzag patterns. The system attempts to recover the original translational symmetry broken by the formation of the rolls [16]. A typical asymptotic configuration of the intensity of the signal field is shown in Fig. 4. Note that this instability first affects transverse wave numbers smaller than the critical one given by (14). We believe that its appearance close to the (unstable) boundary for the generation of spatially homogeneous signal is fortuitous. Further bifurcations to spatiotemporal dynamics still preserve the underlying shape of the roll patterns. For example, for $E=4$ zigzag rolls develop at first with creation and annihilation of dislocations [Fig. 5(A)]. At later times, however, the pattern "freezes" and

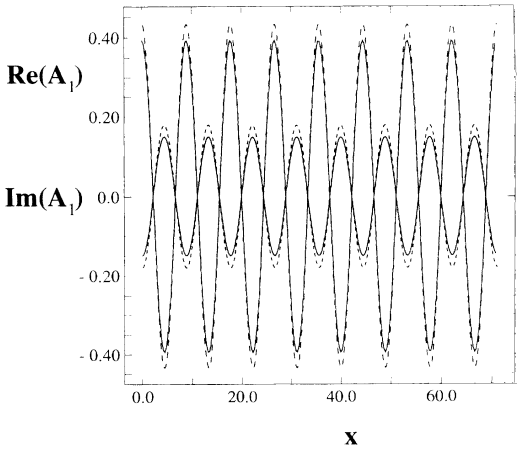

FIG. 2. Comparison between simulations (solid curves) and the analytical form (16)–(20) (dashed curves) for the real (larger amplitude curves) and imaginary part of the OPO signal above the threshold for the formation of rolls. The parameters are the same as in Fig. 1 with $\Delta_0=1.0, a_0=1.0$, and $E=1.5$.

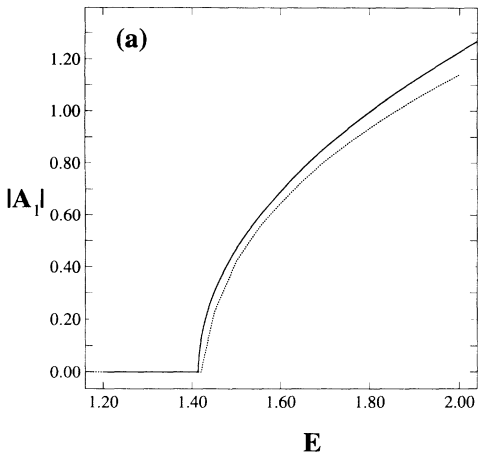

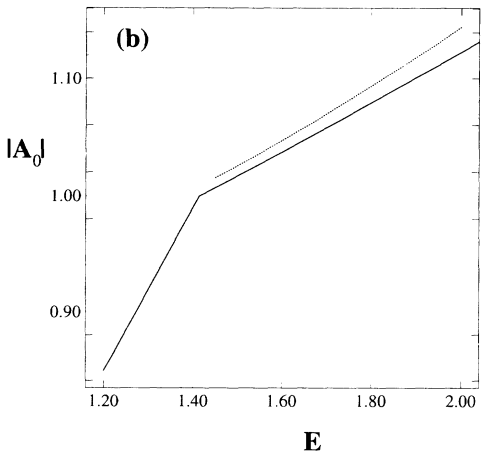

FIG. 3. Comparison between simulations (dashed curves) and the analytical form (16)–(20) (solid curves) for the maximum amplitude of the roll pattern versus the input amplitude E for (a) the OPO signal and (b) the pump field. The parameters are the same as in Fig. 2.

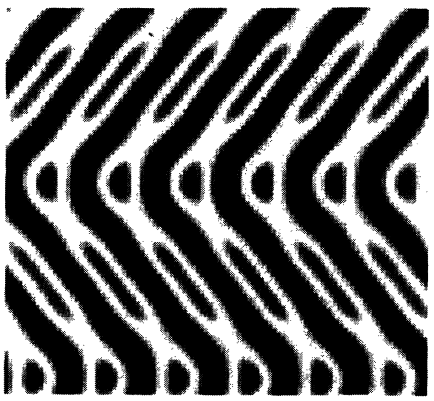

FIG. 4. A stable zigzag configuration of the OPO signal intensity in the transverse plane for $E=2.0$, $\Delta_1=-1.0$, $a_1=1.0$, and the other parameters fixed as in Fig. 2.

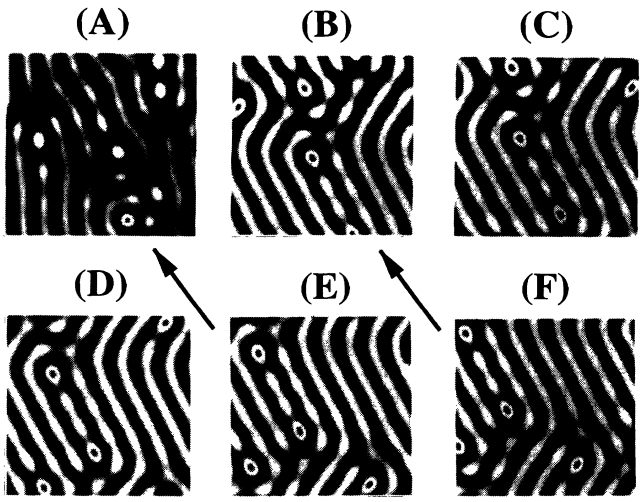

FIG. 5. Time evolution of the transverse OPO signal intensity for $E=4.0$ and the other parameters fixed as in Fig. 4. Time is normalized to the field decay rate and is equal to (A) 250, (B) 22 500, (C) 23 500, (D) 24 000, (E) 24 000, and (F) 24 500, respectively. The arrows show the direction of the scrolling motion in the transverse plane.

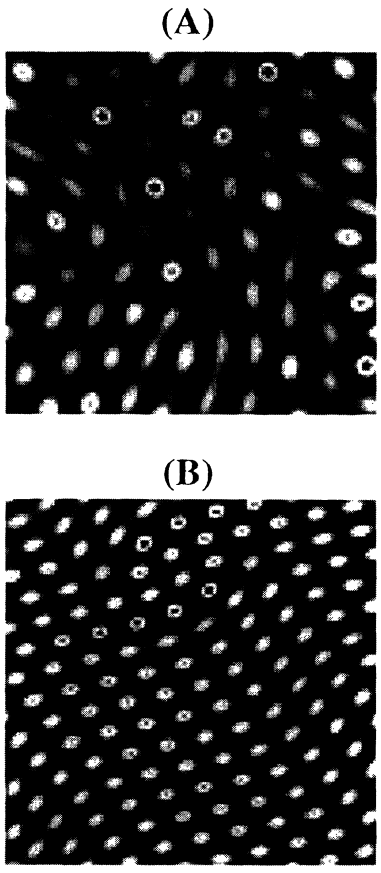

FIG. 6. Transverse configuration of the OPO signal intensity after transients have been discarded, for (A) $E=8.0$, (B) $E=32.0$, and the other parameters fixed as in Fig. 4.

starts to scroll transversally as if it was superposed to a traveling wave [see the time evolution of Figs. 5(B)–5(F)]. We believe that defects of the dislocation type are at least as common in OPO's as optical vortices [9] because of the above specified mechanism for the formation of rolls. Hopf bifurcations, a necessary ingredient for optical vortices, appear for positive values of Δ_1 leading, among other things, to patterns oscillating between two rolls configurations perpendicular to each other. The role, type, and interaction of defects in OPO's are presently under investigation.

We show in Fig. 6(A) that for $E=8$ the initial roll pattern breaks into filaments. For higher values of the input intensity there is a competition between rolls and filaments leading to optical turbulence as the filaments move in an erratic way in the transverse plane [see Fig. 6(B)]. Again, this behavior can be associated with the attempt of the system to recover the spatial symmetries broken by the appearance of the roll patterns.

Finally, for sake of completeness, we present the results of numerical simulations with a nonplanar input beam and show that roll patterns are a robust feature of the system. Figure 7 shows the intensity of the signal in the transverse plane after short-term transients have been discarded. The breaking of the translational symmetry due to the top-hat shape of the input beam results in an orientation of the rolls perpendicular to the circular boundary induced by the input amplitude and in the stabilization of filaments. The spatiotemporal dynamics in the presence of physical shapes of the input laser beam is presently under investigation in order to provide experimentalists with realistic predictions.

In conclusion, we have shown here both analytically and numerically that roll patterns organize the spatiotemporal evolution of OPO's if the detuning parameter Δ_1 of the signal field is negative. For $\Delta_1<0$, diffraction coupled with the nonlinearity of the system allows for an off-axis operation of the OPO with a threshold lower than that predicted by the plane-wave theory. This can be relevant on the experimental side where the input amplitude is a key parameter for the realization of practical devices [1]. The analysis and numerics presented in this paper is not exhaustive of all the spatio-temporal dynamics exhibited by OPO's. For example, the role of different decay rates for the field modes has not been studied and we have focused on negative detunings Δ_1 only. A detailed diagram of the organization and onset of patterns in degenerate and nondegenerate OPO's will be the subject of future work.

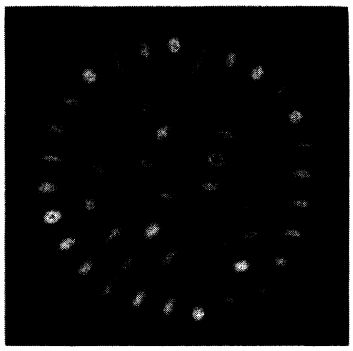

FIG. 7. Transverse configuration of the OPO signal intensity after transients have been discarded, for an input beam of top-hat shape and maximum amplitude equal to 4.0. The other parameters are fixed as in Fig. 4.

We acknowledge financial support from the EEC ESPRIT [Grant No. BR 7118 (TONICS)], SERC (Grants Nos. GR/G/12665 and GR/H/62060), CNR (Grant No. 92.01369.CT02), and NATO (Grant No. 921142).

[1] G. J. Hall, M. Ebrahimzadeh, A. Robertson, G. P. Malcom, and A. I. Ferguson, J. Opt. Soc. Am. B **10**, 2168 (1993).

[2] L.-A. Wu, H. J. Kimble, J. L. Hall, and H. Wu, Phys. Rev. Lett. **57**, 2520 (1986); A. Heidmann, R. Horowicz, S. Reynaud, E. Giacobino, C. Fabre, and G. Camy, *ibid.* **59**, 2555 (1987).

[3] L. A. Lugiato and A. Gatti, Phys. Rev. Lett. **70**, 3868 (1993).

[4] L. A. Lugiato and R. Lefever, Phys. Rev. Lett. **58**, 2209 (1987).

[5] L. A. Lugiato, G.-L. Oppo, J. R. Tredicce, L. M. Narducci, and M. A. Pernigo, J. Opt. Soc. Am. B **7**, 1019 (1990).

[6] W. J. Firth, J. Mod. Opt. **37**, 151 (1990); G. D'Alessandro and W. J. Firth, Phys. Rev. Lett. **66**, 2597 (1991).

[7] J. R. Tredicce, E. J. Quel, A. Chazzawi, C. Green, M. A. Pernigo, L. M. Narducci, and L. A. Lugiato, Phys. Rev. Lett. **62**, 1274 (1989); M. Brambilla, F. Battipede, L. A. Lugiato, V. Penna, F. Prati, C. Tamm, and C. O. Weiss, Phys. Rev. A **43**, 5090 (1991); D. Dangoisse, D. Hennequin, C. Lepers, E. Louvergneaux, and P. Glorieux, *ibid.* **46**, 5955 (1992).

[8] F. T. Arecchi, G. Giacomelli, P. Ramazza, and S. Residori, Phys. Rev. Lett. **65**, 2531 (1990); S. A. Akhmanov, M. A. Vorontsov, V. Y. Ivanov, A. V. Larichev, and N. I. Zheleznykh, J. Opt. Soc. Am. B **9**, 78 (1992).

[9] K. Staliunas, Opt. Commun. **91**, 82 (1992).

[10] P. Coullet, L. Gil, and F. Rocca, Opt. Commun. **73**, 403 (1989); L. Gil, K. Emilsson, and G.-L. Oppo, Phys. Rev. A **45**, 567 (1992); M. Brambilla, M. Cattaneo, L. A. Lugiato, R. Pirovano, F. Prati, A. J. Kent, G.-L. Oppo, A. B. Coates, C. O. Weiss, C. Green, E. J. D'Angelo, and J R. Tredicce, Phys. Rev. A **49**, 1427 (1994).

[11] P. D. Drummond, K. J. McNeil, and D. F. Walls, Opt. Acta **27**, 321 (1980).

[12] L. A. Lugiato, C. Oldano, C. Fabre, E. Giacobino, and R. J. Horowicz, Nuovo Cimento D **10**, 959 (1988); L. A. Lugiato and G. Strini, Opt. Commun. **41**, 67 (1982).

[13] L. Gil, Ph.D. thesis, University of Nice, 1989; P. K. Jakobsen, J. V. Moloney, A. C. Newell, and R. Indik, Phys. Rev. A **45**, 8129 (1992).

[14] L. A. Lugiato, C. Oldano, and L. M. Narducci, J. Opt. Soc. Am. B **5**, 879 (1988).

[15] P. Manneville, *Dissipative Structure and Weak Turbulence* (Academic, San Diego, 1990).

[16] F. Papoff, G. D'Alessandro, G.-L. Oppo, and W. J. Firth, Phys. Rev. A **48**, 634 (1993).

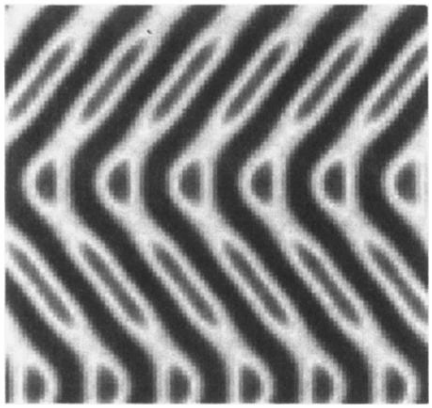

FIG. 4. A stable zigzag configuration of the OPO signal intensity in the transverse plane for $E=2.0$, $\Delta_1=-1.0$, $a_1=1.0$, and the other parameters fixed as in Fig. 2.

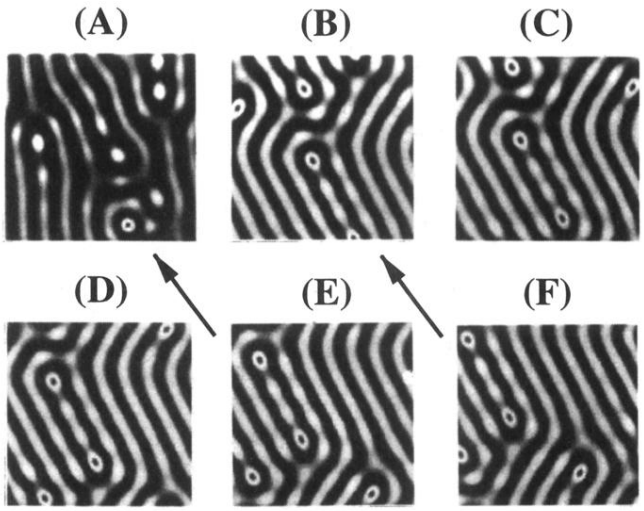

FIG. 5. Time evolution of the transverse OPO signal intensity for $E=4.0$ and the other parameters fixed as in Fig. 4. Time is normalized to the field decay rate and is equal to (A) 250, (B) 22 500, (C) 23 500, (D) 24 000, (E) 24 000, and (F) 24 500, respectively. The arrows show the direction of the scrolling motion in the transverse plane.

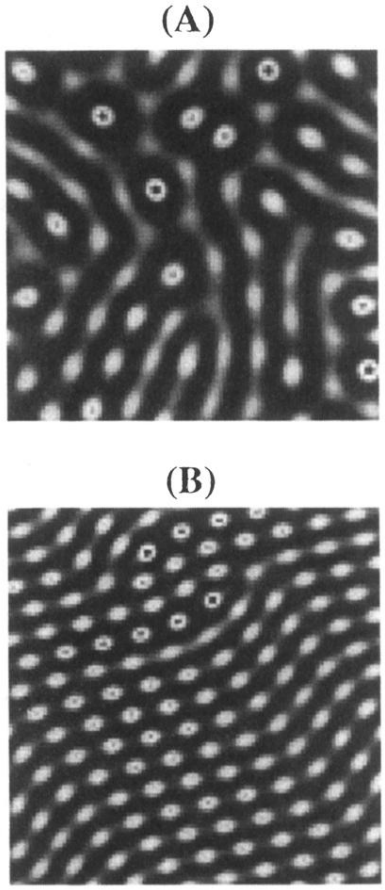

FIG. 6. Transverse configuration of the OPO signal intensity after transients have been discarded, for (A) $E=8.0$, (B) $E=32.0$, and the other parameters fixed as in Fig. 4.

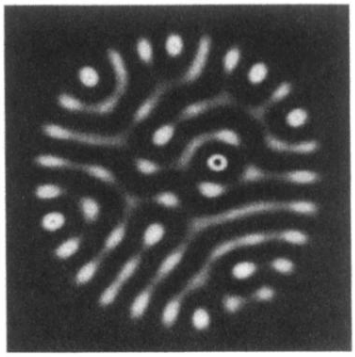

FIG. 7. Transverse configuration of the OPO signal intensity after transients have been discarded, for an input beam of top-hat shape and maximum amplitude equal to 4.0. The other parameters are fixed as in Fig. 4.